iScience

CellPress
OPEN ACCESS

Article

Deep eutectic solvent-assisted fabrication of zirconium phytate thin nanosheets for important biomass transformations

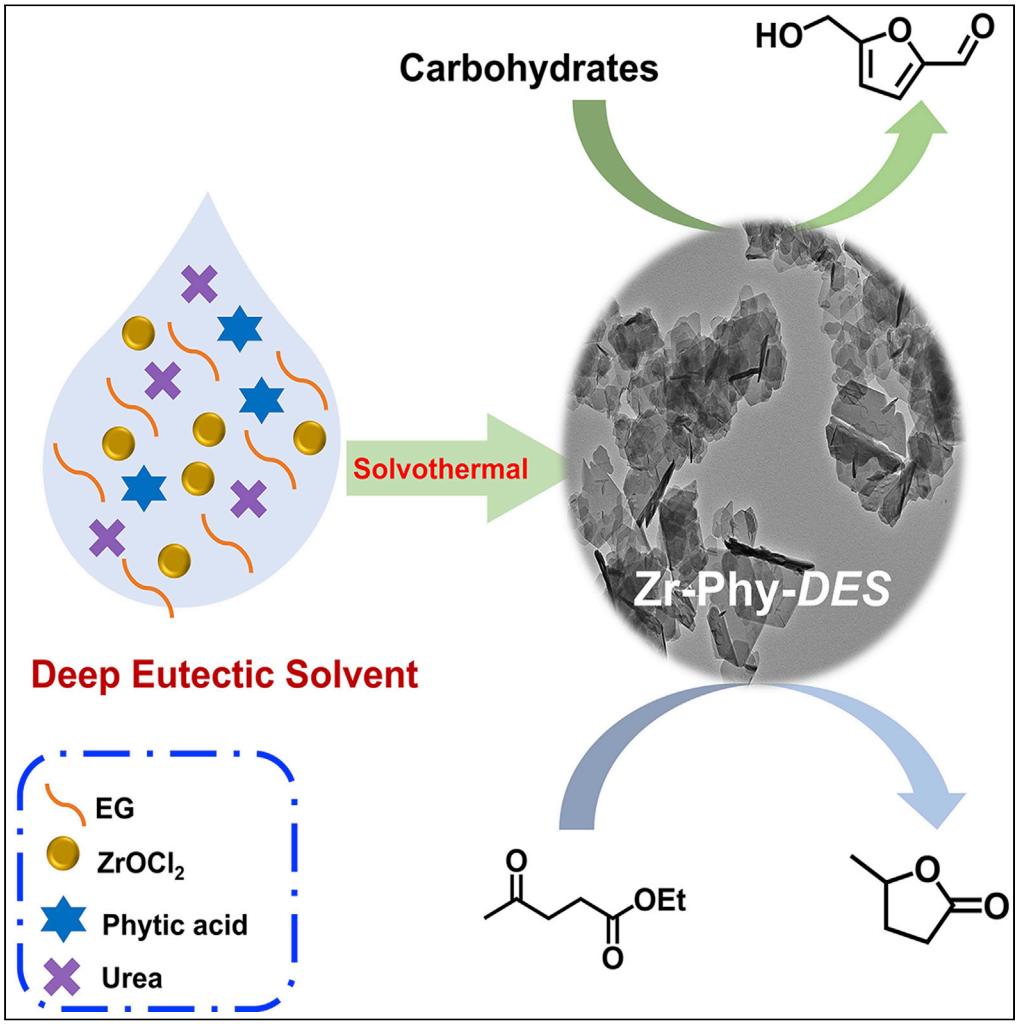

Jinliang Song, Yanan Li, Zhimin Xue

songjl_2021@gdut.edu.cn (J.S.)
zmxue@bjfu.edu.cn (Z.X.)

Highlights

An eco-friendly strategy for preparing catalytic materials with a specific structure

The catalytic activity of the prepared materials varied with the type of solvents

The material prepared in deep eutectic solvent showed better performance

Catalytic materials from natural resources and green solvents to convert biomass

Song et al., iScience 25, 105039
October 21, 2022
https://doi.org/10.1016/j.isci.2022.105039

iScience

CellPress
OPEN ACCESS

Article

Deep eutectic solvent-assisted fabrication of zirconium phytate thin nanosheets for important biomass transformations

Jinliang Song,[1,4,*] Yanan Li,[2] and Zhimin Xue[3,*]

SUMMARY

Utilization of naturally occurring resources to construct functional catalytic materials is significantly important, and facile and environmental-benign strategies are highly desired to afford the materials having a specific structure and good catalytic activity. Herein, we reported an innovative deep eutectic solvent (DES)-assisted strategy to synthesize zirconium phytate with a thin nanosheet structure (denoted as Zr-Phy-*DES*) using plant-originated phytic acid (PhyA) as the renewable building block. This strategy was eco-friendly and adjustable owing to the designability of DESs. The Zr-Phy-*DES* as an acidic catalyst showed high activity on two important biomass transformations, *i.e.*, dehydration of carbohydrates and Meerwein-Ponndorf-Verley reduction of ethyl levulinate. Interestingly, Zr-Phy-*DES* showed higher catalytic performance than the zirconium phytates prepared in ethylene glycol and *N,N*-dimethylformamide, confirming the advantage of DESs for preparing functional materials. Notably, the unique feature of this proposed strategy is that renewable catalysts are prepared in an environmental-benign solvent for efficiently catalyzing biomass transformation.

INTRODUCTION

Fabrication of functional materials using naturally occurring biomass-based resources has been recognized as an important content of green chemistry (Cao et al., 2021; Jin et al., 2021; Maschmeyer et al., 2020; Sahoo et al., 2017; Xiao et al., 2021). The diversity of biomass-based resources in properties and structures provides great potential for the construction of functional materials for specific tasks. In this context, phytic acid (PhyA), naturally occurring polyacids in plants, has attracted significant interest. Traditionally, PhyA has been widely applied in water treatment, protection of metal materials, synthesis of flame retardant, and food industry (Hao et al., 2017; Kumar et al., 2021; Li et al., 2014; Zhang et al., 2018). The unique structure with six phosphate groups (Scheme S1), having the ability to coordinate with diverse metal ions, makes PhyA a promising renewable building block to prepare functional metal phytates (one class of metal phosphonates). Generally, metal phosphonates are acidic materials (Lin et al., 2015; Liu et al., 2020), and thus can be employed as heterogeneous acidic catalysts in some important acid-catalyzed reactions. Undoubtedly, utilization of PhyA as a renewable building block to construct novel metal phytates (M-Phy) as heterogeneous catalysts is significantly attractive.

Despite many advances (Shao et al., 2021; Song et al., 2015, 2018; Wang et al., 2018; Wu et al., 2018; Xue et al., 2016b), the applications of M-Phy in catalysis are still significantly limited by the common drawbacks in heterogeneous catalysis. One of the main challenges is that the heterogeneity can increase the difficulty of the interaction between catalytically active sites and reactants. Besides, the catalytically active sites are partially embedded in the bulk body, resulting in the insufficient utilization of these active sites. Generally, advanced structures, *i.e.*, hierarchically porous structures (Kang et al., 2015; Li et al., 2016), two-dimensional structure (thin nanosheets) (Chen et al., 2022; Hua et al., 2021), and atomic dispersion of active sites (Jones et al., 2016; Yang et al., 2013), can improve the exposion and accessibility of catalytically active sites in heterogeneous catalysts, thus being favorable for heterogeneous catalysis. However, no effort has been devoted to constructing M-Phy with advanced structures for heterogeneous catalysis. Additionally, templates or sacrificial agents are generally involved in most cases of generating the desired advanced structure for heterogeneous catalysts, which makes the processes complex or unbenign on

[1]School of Chemical Engineering and Light Industry, Guangdong University of Technology, Guangzhou 510006, China

[2]College of Environmental Science and Engineering, Taiyuan University of Technology, Taiyuan 030024, China

[3]College of Materials Science and Technology, Beijing Forestry University, Beijing 100083, China

[4]Lead contact

*Correspondence: songjl_2021@gdut.edu.cn (J.S.), zmxue@bjfu.edu.cn (Z.X.)

https://doi.org/10.1016/j.isci.2022.105039

the environment. Therefore, facile, and environment-benign protocols to synthesize M-Phy catalytic materials with advanced structures are in great demand.

Deep eutectic solvents (DESs), an emerging group of green solvents, have drawn significant interest in diverse areas (Chen et al., 2020a; García et al., 2015; Smith et al., 2014; Yu et al., 2021). Owing to the good ability to dissolve a series of organic/inorganic chemicals (Chen et al., 2020b; Jiang et al., 2019; Sun et al., 2022), DESs have been recognized as good solvents for organic reactions and material preparation. More importantly, the hydrogen-bonding networks afford that there are many nanodomains in DESs. The hydrogen-bonding networks and the existing nanodomains can be considered potential templates to synthesize functional materials with advanced structures, thus avoiding the involvement of additive templates or sacrificial agents. Besides, the properties of DESs can be finely and easily tuned to meet the requirement of specific tasks by changing the components of different properties. It is expected that DESs can serve as both the solvent and template to fabricate advanced catalytic materials with controlled morphologies, structures, and properties (Chen et al., 2021; Gállego et al., 2015; Mou et al., 2019).

Inspired by the advantages of DESs in material preparation and the unique property of PhyA, zirconium phytate with a thin nanosheet structure (denoted as Zr-Phy-*DES*) was fabricated by the reaction of PhyA and $ZrOCl_2$ in a DES (EG:urea) composed by ethylene glycol (EG) and urea. As one heterogeneous acidic catalyst, the synthesized Zr-Phy-*DES* exhibited excellent activity for the dehydration of carbohydrates to produce 5-hydroxymethylfurfural (HMF) and Meerwein-Ponndorf-Verley reduction of ethyl levulinate (EL) to generate γ-valerolactone (GVL). Notably, Zr-Phy-*DES* had higher catalytic activity than the materials prepared in EG and *N,N*-dimethylformamide (DMF), confirming the advantage of DESs in constructing advanced catalysts. Outstandingly, the fact of combining green solvents (DESs) and natural compounds (PhyA) to prepare robust catalysts with advanced structures for important biomass transformations enabled this work to be highly promising and practical from a viewpoint of green chemistry. To the best of our knowledge, this was the first work to successfully construct zirconium phytate with a thin nanosheet structure.

RESULTS

Preparation and characterization of Zr-Phy-*DES*

The desired Zr-Phy-*DES* was fabricated via the solvothermal process using PhyA and $ZrOCl_2$ as the precursors in the DES EG:urea with a EG/urea molar ratio of 2:1, and the detailed routes were described in the section of λ method details. Initially, the morphology of Zr-Phy-*DES* was characterized by scanning electron microscopy (SEM) and transmission electron microscopy (TEM). It was observed that the synthesized Zr-Phy-*DES* had a thin nanosheet structure in both SEM (Figure 1A) and TEM images (Figures 1B and S1). Moreover, from the image of high-resolution TEM (HR-TEM), Zr-Phy-*DES* possessed plenty of mesopores (Figure S2), and elemental distribution mapping (Figure S3) showed that three elements (*i.e.*, Zr, P, and O) dispersed uniformly in the fabricated Zr-Phy-*DES*. For comparison, two other zirconium phytates were also prepared using EG and DMF as the solvents with one similar route of preparing Zr-Phy-*DES*, and these two materials were denoted as Zr-Phy-*EG* and Zr-Phy-*DMF*. As characterized by SEM and TEM, Zr-Phy-*EG* and Zr-Phy-*DMF* showed significantly different morphology from Zr-Phy-*DES*. Zr-Phy-*EG* had a poorer (thicker and smaller in size) nanosheet-like structure (Figures 1C and 1D) in comparison with Zr-Phy-*DES*, while Zr-Phy-*DMF* showed irregular morphology (Figures 1E and 1F). Additionally, these results above indicated that protic solvents (*e.g.*, DESs and EG) were beneficial for generating the nanosheet structure, while aprotic polar solvents (*e.g.*, DMF) did not favor the formation of nanosheets. Zr-Phy-*DES* had a much thinner nanosheet than Zr-Phy-*EG*, which was probably caused by the good performance of DESs on the exfoliation and dispersion of 2D materials (Abdelkader et al., 2015; Abdelkader and Kinloch, 2016; Sang et al., 2021; Tan et al., 2018).

Power X-ray diffraction (XRD) patterns (Figure 2A) of all the three materials (*i.e.*, Zr-Phy-*DES*, Zr-Phy-*EG*, and Zr-Phy-*DMF*) only showed two broad peaks, indicating that all the obtained three materials had low crystallinity. Besides, similar the FT-IR spectra of the three zirconium phytates were also similar (Figure 2B), and a sharp band around 1100 cm^{-1} was observed in their FT-IR spectra, which corresponded to the Zr-*O*-P stretching vibrations (Li et al., 2018a; Lin et al., 2015), while this band was not observed for ZrO_2, implying the formation of Zr-*O*-P networks in Zr-Phy-*DES*, Zr-Phy-*EG*, and Zr-Phy-*DMF*. As determined by the N_2 adsorption-desorption technique (Figure 2C), the Zr-Phy-*DES* had a well-defined mesoporous structure, which was consistent with the results of the HR-TEM examination (Figure S2), and its BET surface area

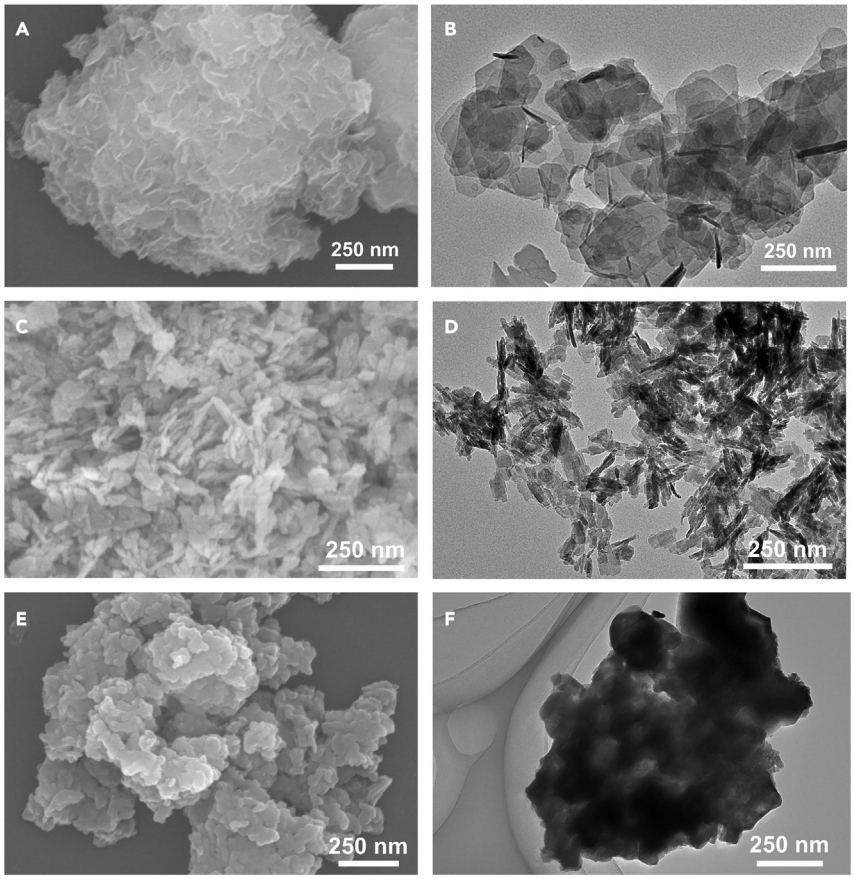

Figure 1. The morphology of the zirconium phytates prepared in different solvents

(A–F) SEM (A, C, and E) and TEM (B, D, and F) images of the synthesized zirconium phytates. Zr-Phy-*DES* (A, and B), Zr-Phy-*EG* (C, and D), and Zr-Phy-*DMF* (E, and F).

was 254.6 m^2/g (Table S1). In comparison, although Zr-Phy-*EG* and Zr-Phy-*DMF* also possessed the mesoporous structure, but their surface areas were lower than that of Zr-Phy-*DES* (Table S1), probably resulting from the larger hydrogen-bonding networks in the DES. X-ray photoelectron spectroscopy (XPS) showed the characteristic binding energies of Zr^{4+} (Zr $3d_{3/2}$, about 186.2 eV, and Zr $3d_{5/2}$, 183.8 eV) and P^{5+} (P 2p, about 134.4 eV) in the three materials (Figures 2D and 2E), which were consistent with the reported values for zirconium phosphonate (Song et al., 2015; Zhou et al., 2017), implying that the constructed zirconium phytates in all the three solvents were probably one kind of zirconium phosphonate (zirconium phytates). Additionally, as determined by ICP and elemental analysis, the contents of Zr, P, and C in Zr-Phy-*DES*, Zr-Phy-*EG*, and Zr-Phy-*DMF* were similar (Table S2), implying that solvents could not affect the material composition. Thus, the molar ratio of Zr and P in the synthesized three materials was about 0.5, suggesting that one Zr^{4+} coordinated with two phosphate groups. Based on these results and the structure of PhyA, the most ideal connectivity pattern in the three zirconium phytates was provided in Figure S4. However, the fact that one Zr^{4+} could coordinate with two phosphate groups in the same PhyA molecule or two different molecules made much irregular connectivity exist in the obtained materials, which resulted in the inferior crystallinity (Figure 2A) and the irregular size of particle or nanosheets (Figures 1A and 1B).

As discussed above, Zr-Phy-*DES* has higher surface area than both Zr-Phy-*EG* and Zr-Phy-*DMF*. Simultaneously, an obvious thin-nanosheet structure was observed for Zr-Phy-*DES* in comparison with the structures of Zr-Phy-*EG* and Zr-Phy-*DMF*. Both the higher surface area and the better nanosheet structure were beneficial for the exposion and accessibility of catalytic active sites to interact with the reactants. Thereby, Zr-Phy-*DES* would be potentially more efficient than Zr-Phy-*EG* and Zr-Phy-*DMF* for some important reactions, which would be discussed in the following sections.

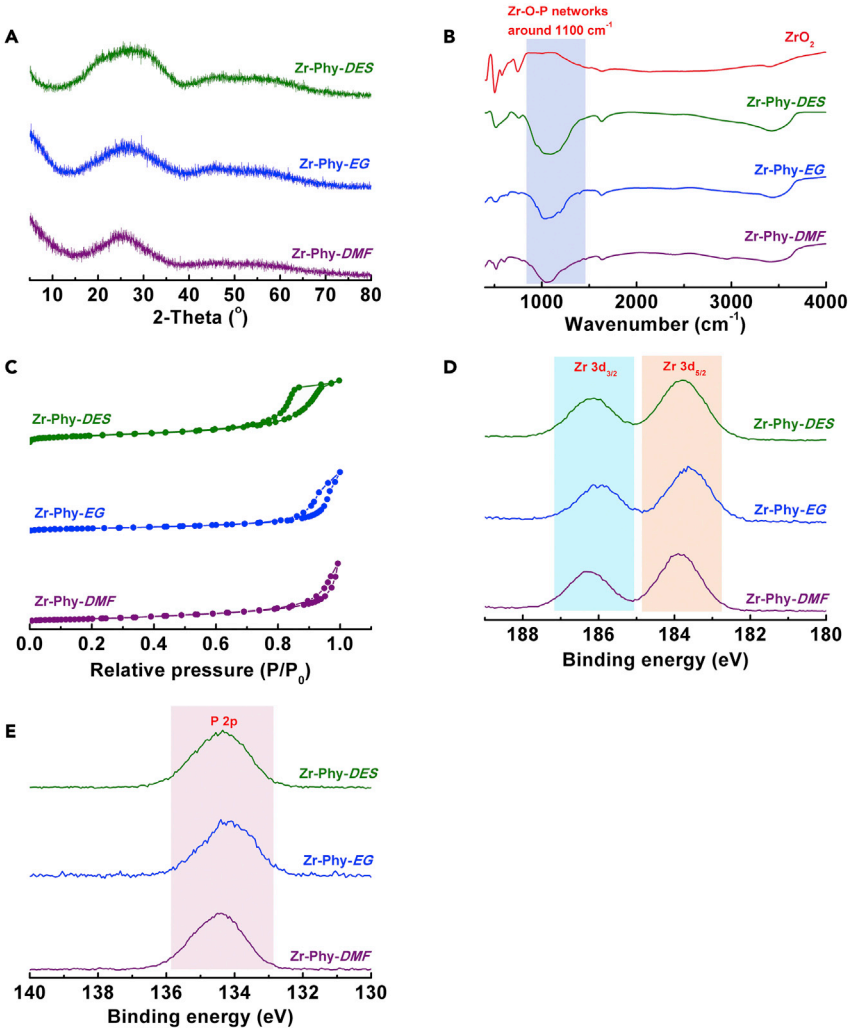

Figure 2. Characterization of the synthesized zirconium phytates

(A–E) (A) XRD patterns, (B) FT-IR spectra, (C) N_2 adsorption-desorption isotherms, (D) XPS spectra of Zr 3days, and (E) XPS spectra of P 2p.

Dehydration of carbohydrates

Production of 5-hydroxymethylfurfural (HMF) via dehydration of carbohydrates has attracted significant attention in the past decade (Wang et al., 2017; Xu et al., 2020; Zhao et al., 2007) because HMF has been recognized as a versatile biomass-based platform compound for synthesizing diverse valuable chemicals (Kisszekelyi et al., 2020; Li et al., 2021; Sajid et al., 2018; Wang et al., 2014; Zhang et al., 2020). Generally, a suitable acidic catalyst is essential to promote the dehydration of carbohydrates. As described above, zirconium phytate is a type of acidic materials. Thus, we attempted to utilize the synthesized zirconium phytates as acidic catalysts for the dehydration of several carbohydrates (*i.e.*, fructose, inulin, and sucrose) to produce HMF in 1-butyl-3-methylimidazolium chloride ([Bmim]Cl, an ionic liquid), with the purpose of verifying the advantage of DESs on constructing robust catalytic materials. In this reaction system, both the zirconium phytates and the [Bmim]Cl played a significant role in the dehydration. First, as well-accepted, [Bmim]Cl acting as an effective solvent could significantly decrease the overall barrier of the dehydration process by the solvation of the fructose molecules via the formation of hydrogen bonding between the hydroxy groups in the carbohydrates and the chloride ions of [Bmim]Cl (Li et al., 2019; Xiao and Song, 2014; Zhao et al., 2007), thus promoting the dehydration of carbohydrates. Second, the solid catalysts (*i.e.*, Zr-Phy-*DES*, Zr-Phy-*EG*, and Zr-Phy-*DMF*) played the role of providing suitable acidic sites (mainly the Zr Lewis acidic sites) to catalyze the removal of H_2O molecules from the

Table 1. Dehydration of various carbohydrates to HMF over different catalysts[a]

Entry	Carbohydrate	Catalyst	Conversion (%)[b]	Yield (%)[b]
1	Fructose	None	16.9	13.3
2	Fructose	Zr-Phy-*DES*	100	91.6
3	Fructose	Zr-Phy-*EG*	93.7	84.2
4	Fructose	Zr-Phy-*DMF*	91.2	80.4
5	Fructose	ZrO_2	35.1	27.8
6[c]	Fructose	Zr-Phy-*DES*	95.2	86.5
7	Sucrose	Zr-Phy-*DES*	100	47.3
8	Sucrose	Zr-Phy-*EG*	89.2	40.9
9	Sucrose	Zr-Phy-*DMF*	81.7	38.2
10[d]	Inulin	Zr-Phy-*DES*	–	63.7
11[d]	Inulin	Zr-Phy-*EG*	–	55.3
12[d]	Inulin	Zr-Phy-*DMF*	–	50.1
13	Glucose	Zr-Phy-*DES*	23.3	<3

[a]Reaction conditions: carbohydrate, 0.1 g; catalyst, 0.05 g; [Bmim]Cl, 1 g; reaction temperature, 100 °C; reaction time, 2 h for fructose and glucose, 4 h for sucrose, or 5 h for inulin.
[b]The conversions and the actual HMF amount were determined by HPLC using an external standard method, and the theoretical HMF amount were calculated based on the amount of monosaccharide unit in the corresponding carbohydrate. Then, the HMF yield was calculated based on the ratio of actual HMF amount and theoretical HMF amount.
[c]Zr-Phy-*DES* was recycled for the fifth run.
[d]The conversion of inulin was not determined owing to its polymer nature.

carbohydrate molecule (Eminov et al., 2014; Ma et al., 2017; Xie et al., 2012) via the interaction between the O atom of the hydroxy groups in the carbohydrates and the acidic sites, which followed a classic mechanism for alcohol dehydration (Pfriem et al., 2021; Yang et al., 2020). The synergistic effect of solid catalysts with appropriate acidic sites and [Bmim]Cl could enable the dehydration of carbohydrates (*i.e.*, fructose, inulin, and sucrose) to be conducted efficiently to produce HMF.

Initially, dehydration of fructose was selected as a model reaction to evaluate the catalytic activity of various catalysts (Table 1). A very low yield of HMF (13.3%) was achieved in the catalyst-free system (Table 1, entry 1), implying the slow reaction rate of autocatalysis, which confirmed that suitable catalysts were required to promote the dehydration. In comparison, the synthesized zirconium phytates in different solvents could significantly enhance the formation of HMF from fructose dehydration (Table 1, entries 2-4), and Zr-Phy-*DES* provided the highest catalytic activity with the complete conversion of fructose and an HMF yield of 91.6% (Table 1, entry 2). Additionally, ZrO_2 showed very poor activity for the reaction (Table 1, entry 5). These results indicated that Zr-Phy-*DES* showed the highest catalytic activity for the dehydration of fructose among the examined catalysts, and the reason would be discussed later in discussion. Expect for fructose, the catalytic performance of Zr-Phy-*DES* on the dehydration of inulin and sucrose was also investigated. Obviously, the catalytic activity of Zr-Phy-*DES* was still higher than that of Zr-Phy-*EG* or Zr-Phy-*DMF* (Table 1, entries 7-12), further confirming the advantage of DES for the preparation of robust catalytic materials. The varied HMF yield from fructose, inulin, and sucrose and their different reactivity are probably caused by their different molecular structures (Scheme S2). A hydrolysis step was necessary for inulin (one polymer) and sucrose (one disaccharide), which would decrease the rate of converting these two carbohydrates to generate HMF. Besides, very low yield of HMF (<3%) was generated from the dehydration of glucose over Zr-Phy-*DES* although the conversion of glucose could reach 23.3% (Table 1, entry 13), indicating that glucose preferred to be converted into some by-products rather than HMF in our catalytic system under the investigated reaction conditions. Thereby, we could deduce that the glucose units in inulin and sucrose could not be selectively converted into the desired HMF but some by-products, which resulted in the lower yields of HMF from inulin and sucrose because the yields were calculated by considering the amount of all monosaccharide units in the examined carbohydrates.

Subsequently, the reaction parameters (*i.e.*, reaction temperature, catalyst usage, and reaction time) were optimized using Zr-Phy-*DES* as the catalyst. As expected, reaction temperature significantly affected the

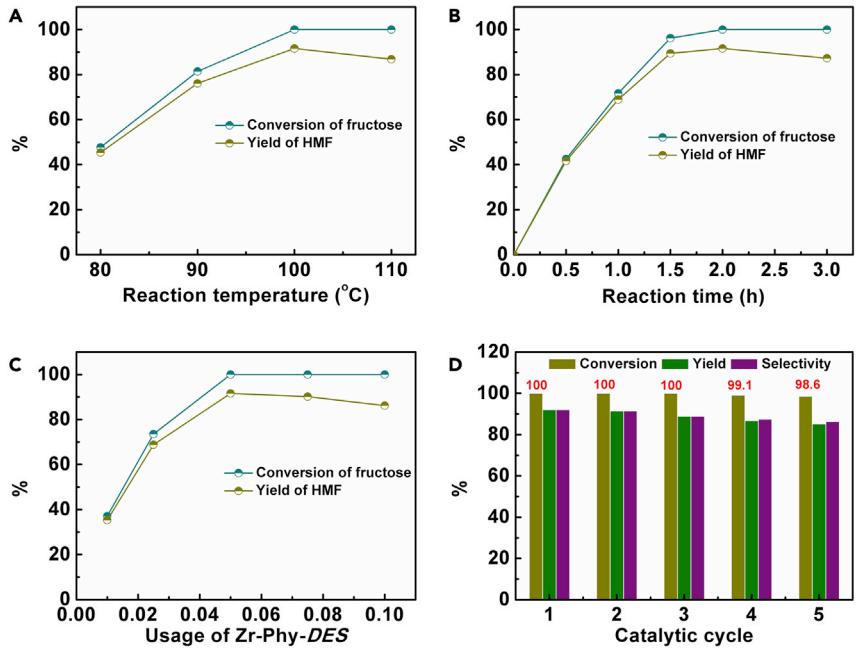

Figure 3. Optimization of reaction conditions for dehydration of fructose

(A–D) (A) Effect of reaction temperature, (B) Influence of reaction time, (C) Effect of Zr-Phy-*DES* usage, and (D) Recyclability of Zr-Phy-*DES*/[Bmim]Cl catalytic system. Reaction conditions: fructose, 0.1 g; [Bmim]Cl, 1 g; Zr-Phy-*DES*, 0.05 g for A, B, and D; reaction temperature, 100 °C for B-D; reaction time, 2 h for A, C, and D.

reaction efficiency (Figure 3A). The fructose conversion and HMF yield increased when the reaction temperature increased from 80 to 100 °C, and fructose could be completely converted with an HMF yield of 91.6% at 100 °C. However, when the reaction temperature was further improved to 110 °C, the yield of HMF slightly decreased owing to that more HMF were decomposed at higher reaction temperature. Thus, 100 °C was the optimized reaction temperature for our catalytic system. Kinetic investigation revealed that the suitable reaction time was 2 h (Figure 3B). Too long reaction time would result in the decomposition of the generated HMF. Moreover, the yield of HMF increased firstly when the Zr-Phy-*DES* usage increased from 0.01 to 0.05 g Figure 3C), and then decreased with a Zr-Phy-*DES* usage of more than 0.05 g. More usage of Zr-Phy-*DES* not only promoted the dehydration of fructose but also enhanced the decomposition of the generated HMF. These two opposite effects made 0.05 g the optimized catalyst usage under our reaction conditions. Finally, Zr-Phy-*DES* could be reused for five catalytic cycles without a considerable decrease in catalytic performance (Table 1, entry 6 and Figure S5), and the slight decrease in catalytic activity may be caused by the loss of Zr-Phy-*DES* in the recovery process. As characterized by TEM (Figure S6), N_2 adsorption-desorption method (Table S1), and NH_3-TPD (Table S3), no difference was observed between the fresh Zr-Phy-*DES* and the recovered one, indicating the stability of Zr-Phy-*DES* under the reaction conditions. More importantly, the catalytic activity of Zr-Phy-*DES*/[Bmim]Cl showed no obvious decrease in five catalytic cycles (Figure 3D), verifying the stability of the whole catalytic system.

As well-accepted, acidity plays a crucial role in the dehydration of various carbohydrates (*i.e.*, fructose, inulin, and sucrose) to produce HMF. Thus, the acidity of various catalysts was determined by NH_3-TPD (Table S3). Obviously, Zr-Phy-*DES* had much higher acidity than Zr-Phy-*EG*, Zr-Phy-*DMF*, and ZrO_2. These results were probably caused by the higher surface area and the thin nanosheet structure of Zr-Phy-*DES*, which both favored the exposion of the acidic sites. Based on the results in Table 1, the catalytic activity of different catalysts was positively correlated with their acidity (Figure 4). Zr-Phy-*DES* with the strongest acidity showed the highest catalytic activity. Except for increasing the acidity of Zr-Phy-*DES*, the highest surface area and thin nanosheet structure could improve the accessibility of acidic sites by the carbohydrate molecule. In comparison, the thicker nanosheets of Zr-Phy-*EG* resulted in a decrease in utilization efficiency of acidic sites, and its lower surface area increased the difficulty of the interaction between acidic sites and the carbohydrate molecule. The bulk structure of Zr-Phy-*DMF* made the utilization efficiency of its acidic sites be lowest, and the accessibility of acidic sites in Zr-Phy-*DMF* by the carbohydrate molecule was

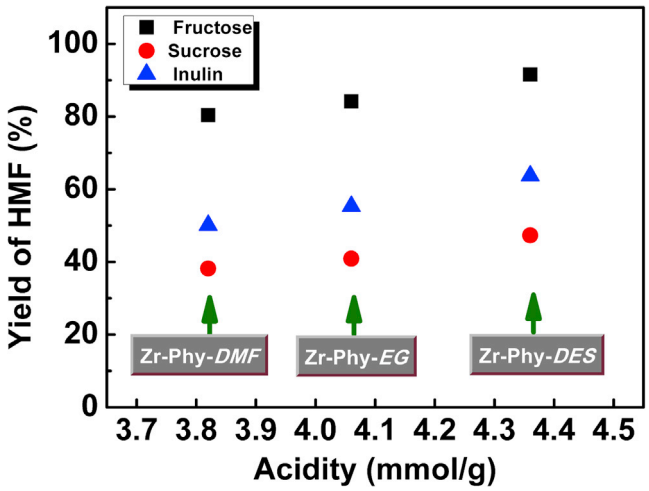

Figure 4. The correlation between the catalytic activity and the acidity

weakest owing to its lowest surface area among the three materials. From the discussion above, the catalytic performance of the prepared zirconium phytates on the dehydration of carbohydrates showed a positive relationship with their surface area and structures. The highest surface area and thin nanosheet structure afforded Zr-Phy-*DES* having the highest catalytic activity for the dehydration of various carbohydrates to produce HMF among the synthesized three materials.

Meerwein-Ponndorf-Verley reduction of biomass-derived ethyl levulinate

Ethyl levulinate (EL) is an important type of biomass platform compounds. Upgrading EL into various valuable chemicals has attracted significant attention (He et al., 2021; Luo et al., 2015; Xie et al., 2019). In this regard, Meerwein-Ponndorf-Verley (MPV) reduction of EL to produce γ-valerolactone (GVL) has been recognized as one of the most promising strategies (Scheme S3). Of the developed catalysts, Zr-contained materials are the most investigated type for MPV reduction of EL (Li et al., 2018b; Kuwahara et al., 2017; Song et al., 2015; Wang et al., 2022). In our previous work (Song et al., 2015), zirconium phytate has been utilized as an effective catalyst for MPV reduction of EL to synthesize GVL. However, the zirconium phytate in this previous work did not possess a specific structure, and its catalytic activity needed to be further enhanced. Because the Zr-Phy-*DES* showed a unique structure (thin nanosheets), we assumed that Zr-Phy-*DES* probably had enhanced catalytic activity on the MPV reduction of EL. Thereby, MPV reduction of biomass-derived EL was also employed to further confirm whether DESs have an advantage in fabricating robust catalytic materials or not (Table 2).

No reaction occurred in the absence of any catalysts (Table 2, entry 1), indicating that a suitable catalyst was essential for the MPV reduction of EL. Subsequently, it was observed that the synthesized three zirconium phytates (*i.e.*, Zr-Phy-*DES*, Zr-Phy-*EG*, and Zr-Phy-*DMF*) could catalyze the MPV reduction of EL (Table 2, entries 2-7), and Zr-Phy-*DES* still exhibited the best catalytic performance at 130 °C (Table 2, entries 4 and 7). More importantly, the catalytic activity increased with the following order: Zr-Phy-*DMF* < Zr-Phy-*EG* < Zr-Phy-*DES*, which was consistent with the tendency for the dehydration of carbohydrates. Besides, isopropyl levulinate as the by-product was detected in all reactions because the steric hindrance of the isopropyl group resulted in its lower reactivity to further be converted into GVL. The lowest yield of isopropyl levulinate over Zr-Phy-*DES* was probably caused by its highest catalytic activity on the MPV reduction of levulinate esters. These results further verified the fact that DESs had the unique advantage in the preparation of robust catalytic materials. Additionally, for the MPV reduction of EL, Zr-Phy-*DES* could be recycled at least for five runs without an obvious decrease in catalytic activity and product selectivity (Table 2, entry 8), suggesting the good stability of Zr-Phy-*DES*. We also characterized the recovered Zr-Phy-*DES* from MPV reduction by several techniques, including TEM (Figure S7), N_2 adsorption-desorption method (Table S1), and CO_2-TPD (Table S4). It was observed that there were no significant changes in the properties of the recovered Zr-Phy-*DES* in comparison with the virgin material, implying the good stability of Zr-Phy-*DES* in the MPV reduction under our reaction conditions.

Table 2. MPV reduction of EL to produce GVL over different catalysts[a]

Entry	Reactant	Catalyst	Time (h)	Conversion (%)[b]	GVL Yield (%)[b]
1	EL	None	6	0	0
2	EL	Zr-Phy-*EG*	6	98.7	91.6
3	EL	Zr-Phy-*DMF*	6	93.2	81.3
4	EL	Zr-Phy-*DES*	6	99.2	96.8
5	EL	Zr-Phy-*EG*	3	89.1	66.4
6[c]	EL	Zr-Phy-*DMF*	3	77.3	54.5
7	EL	Zr-Phy-*DES*	3	97.3	74.7
8[days]	EL	Zr-Phy-*DES*	6	98.8	95.4

[a]Reaction conditions: EL, 1 mmol; catalyst, 0.2 g; isopropanol, 5 g; reaction temperature, 130 °C.
[b]The conversions and yields were determined by GC using cyclohexanol as the internal standard.
[c]Zr-Phy-*DES* was reused for the fifth cycle.

As is well-accepted, the electronic state of Zr species significantly affected the activity of Zr-containing catalysts on the MPV reduction of EL (Song et al., 2015; Wang et al., 2022). Therefore, XPS spectra were performed to characterize the electronic state of Zr species in Zr-Phy-*DES*, Zr-Phy-*EG*, and Zr-Phy-*DMF*. As shown in Figure S8, the difference in the binding energies of Zr species in these three materials was not significant. Besides, the basicity generally has an impact on the catalytic activity, and thus we examined the basicity of the three zirconium phytates by CO_2-TPD (Table S4). However, the slight difference in basicity could not result in such obvious difference in catalytic activity (Table 2). From these discussions, we could deduce that the electronic state of Zr species and the basicity were not the crucial parameters on the catalytic activity of the zirconium phytates in synthesized different solvents. Probably, the highest surface area and the thin nanosheet structure of Zr-Phy-*DES* enhanced the exposion of catalytically active sites (Zr species and basic sites), thereby improving their accessibility by the EL molecule. Therefore, Zr-Phy-*DES* possessed the best catalytic performance for the MPV reduction of EL among the synthesized zirconium phytates. Additionally, the catalytic performance of Zr-Phy-*DES*, Zr-Phy-*EG*, and Zr-Phy-*DMF* on the MPV reduction of EL was also positively correlated with their surface area and structures, which was consistent with the results for the dehydration of carbohydrates over these materials.

Based on some previously reported knowledge (Song et al., 2015; Xue et al., 2016a; Kuwahara et al., 2017; Wang et al., 2022), MPV reduction over Zr-containing catalysts proceeded via a concerted process involving a six-link intermediate. Herein, we proposed a reasonable catalytic mechanism for the MPV reduction of EL over Zr-Phy-*DES* (Scheme 1). In the catalytic cycle, the Zr sites in the Zr-Phy-*DES* played the role of activating the carbonyl group in EL by the interaction between the O atom of the carbonyl group and the Zr site. Simultaneously, the hydroxyl group in isopropanol was activated acid-base pair (Zr^{4+}-O^{2-}) in Zr-Phy-*DES*. Subsequently, the hydrogen in the activated hydroxyl group was transferred to the activated carbonyl group of EL via a six-link intermediate, and ethyl 4-hydroxypentanoate (EHP) would be generated through this process. Finally, GVL was formed by the intramolecular transesterification of ethyl 4-hydroxypentanoate promoted by the acidic or basic sites on Zr-Phy-*DES*. In the reaction process, the involved isopropanol was transformed into acetone.

DISCUSSION

In conclusion, we successfully fabricated zirconium phytate (Zr-Phy-*DES*) with a thin nanosheet structure using phytic acid as a renewable building block via a solvothermal process in the DES formed by EG and urea. It was observed that the properties of the synthesized zirconium phytates correlated with the involved solvents, thus affecting their catalytic activity. Interesting, the catalytic activity of Zr-Phy-*DES* on the dehydration of carbohydrates to HMF and MPV reduction of EL to GVL was higher than those of Zr-Phy-*EG* and Zr-Phy-*DMF*, which confirmed the advantage of DESs to construct functional materials. Systematic investigation revealed that Zr-Phy-*DES* had higher surface area and a thin nanosheet, which favored the exposion and accessibility of catalytically active sites, thus promoting both transformations. We believe that Zr-Phy-*DES* has great potential for application in the dehydration of carbohydrates to produce HMF and MPV reduction of EL to generate GVL, and other robust catalysts with specific structure can be designed by combining green DESs and naturally occurring resources for biomass valorization.

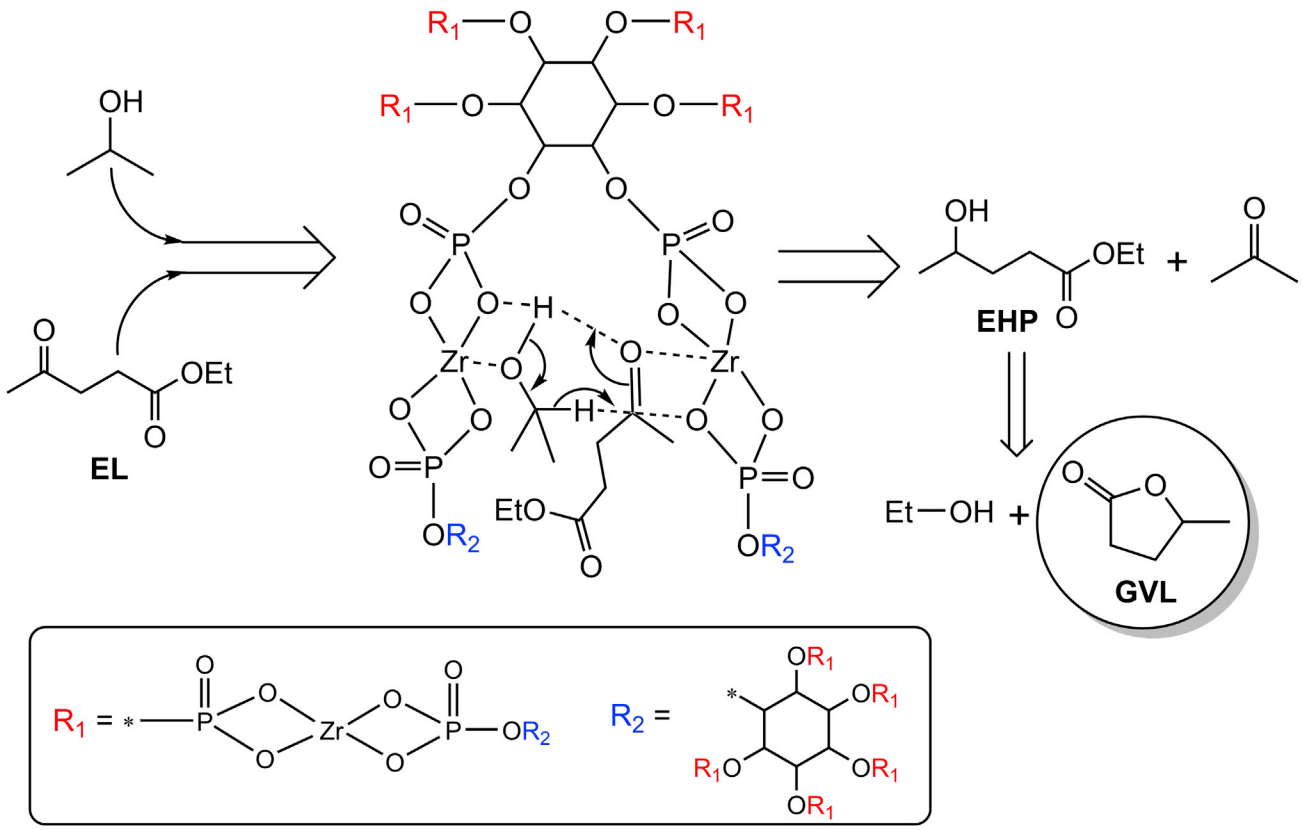

Scheme 1. The possible catalytic mechanism for Zr-Phy-*DES*-catalyzed MPV reduction of EL to produce GVL

Limitations of the study

By the DES-assisted strategy, we successfully synthesized zirconium phytate thin nanosheets using naturally occurring phytic acid as the building block. Meanwhile, the zirconium phytate synthesized in DES showed better performance on two important biomass transformations. Nevertheless, this study only confirmed the feasibility of utilizing DES to tune the properties of functional materials, especially those from renewable resources. We feel that more tasks, *i.e.*, effect of DES types, the interaction between the DES and the precursors, the influence of varied preparation parameters (temperature, and time), and molecular simulation, needed to be performed, and these tasks may be helpful for revealing the mechanism of forming specific structure in DESs at the molecular level. However, such tasks have not been fulfilled, and are ongoing in our lab.

STAR★METHODS

Detailed methods are provided in the online version of this paper and include the following:

- KEY RESOURCES TABLE
- RESOURCE AVAILABILITY
  - Lead contact
  - Materials availability
  - Data and code availability
- METHOD DETAILS
  - Preparation of the desired DES (EG:Urea-2:1)
  - Synthesis of Zr-Phy-*DES*, Zr-Phy-*EG*, and Zr-Phy-*DMF*
  - Catalyst characterization
  - Dehydration of various carbohydrates
  - MPV reduction of EL

SUPPLEMENTAL INFORMATION

Supplemental information can be found online at https://doi.org/10.1016/j.isci.2022.105039.

ACKNOWLEDGMENTS

This work was financially supported by the National Natural Science Foundation of China (22072157, and 21873012).

AUTHOR CONTRIBUTIONS

J.S., and Z.X. proposed the project, designed the experiments, and wrote the article. J.S. performed the whole experiments. Y.L. and Z.X. performed the analysis of experimental data. All authors discussed the results and commented on the article.

DECLARATION OF INTERESTS

The authors declare no competing interests.

INCLUSION AND DIVERSITY

We support inclusive, diverse, and equitable conduct of research.

Received: May 18, 2022
Revised: July 26, 2022
Accepted: August 24, 2022
Published: October 21, 2022

REFERENCES

Abdelkader, A.M., and Kinloch, I.A. (2016). Mechanochemical exfoliation of 2D crystals in deep eutectic solvents. ACS Sustainable Chem. Eng. *4*, 4465–4472. https://doi.org/10.1021/acssuschemeng.6b01195.

Abdelkader, A.M., Patten, H.V., Li, Z., Chen, Y., and Kinloch, I.A. (2015). Electrochemical exfoliation of graphite in quaternary ammonium-based deep eutectic solvents: a route for the mass production of graphene. Nanoscale *7*, 11386–11392. https://doi.org/10.1039/c5nr02840j.

Cao, S., Rathi, P., Wu, X., Ghim, D., Jun, Y.-S., and Singamaneni, S. (2021). Cellulose nanomaterials in interfacial evaporators for desalination: a "natural" choice. Adv. Mater. *33*, 2000922. https://doi.org/10.1002/adma.202000922.

Chen, B., He, C., Cao, M., Qiu, X., Ouyang, X., and Qian, Y. (2022). Fabricating nickel phyllosilicate-like nanosheets to prepare a defect-rich catalyst for the one-pot conversion of lignin into hydrocarbons under mild conditions. Green Chem. *24*, 846–857. https://doi.org/10.1039/d1gc03909a.

Chen, T., Ying, H., Zhang, C., Bi, J., Li, Z., and Hao, J. (2021). Engineering an Fe_2O_3/FeS hybrid catalyst from a deep eutectic solvent for highly efficient electrocatalytic N_2 fixation. Chem. Commun. *57*, 6688–6691. https://doi.org/10.1039/d1cc02072b.

Chen, Y., Han, X., Liu, Z., Yu, D., Guo, W., and Mu, T. (2020a). Capture of toxic gases by deep eutectic solvents. ACS Sustainable Chem. Eng. *8*, 5410–5430. https://doi.org/10.1021/acssuschemeng.0c01493.

Chen, Y., Lu, Y., Liu, Z., Zhou, L., Li, Z., Jiang, J., Wei, L., Ren, P., and Mu, T. (2020b). Efficient dissolution of lithium-ion batteries cathode $LiCoO_2$ by polyethylene glycol-based deep eutectic solvents at mild temperature. ACS Sustainable Chem. Eng. *8*, 11713–11720. https://doi.org/10.1021/acssuschemeng.0c03624.

Eminov, S., Wilton-Ely, J.D.E.T., and Hallett, J.P. (2014). Highly selective and near-quantitative conversion of fructose to 5-hydroxymethylfurfural using mildly acidic ionic liquids. ACS Sustainable Chem. Eng. *2*, 978–981. https://doi.org/10.1021/sc400553q.

Gállego, I., Grover, M.A., and Hud, N.V. (2015). Folding and imaging of DNA nanostructures in anhydrous and hydrated deep-eutectic solvents. Angew. Chem. Int. Ed. *54*, 6765–6769. https://doi.org/10.1002/anie.201412354.

García, G., Aparicio, S., Ullah, R., and Atilhan, M. (2015). Deep eutectic solvents: physicochemical properties and gas separation applications. Energy Fuels *29*, 2616–2644. https://doi.org/10.1021/ef5028873.

Hao, Y., Sani, L.A., Ge, T., and Fang, Q. (2017). Phytic acid doped polyaniline containing epoxy coatings for corrosion protection of Q235 carbon steel. Appl. Surf. Sci. *419*, 826–837. https://doi.org/10.1016/j.apsusc.2017.05.079.

He, J., Wu, Z., Gu, Q., Liu, Y., Chu, S., Chen, S., Zhang, Y., Yang, B., Chen, T., Wang, A., et al. (2021). Zeolite-tailored active site proximity for the efficient production of pentanoic biofuels. Angew. Chem. Int. Ed. *60*, 23713–23721. https://doi.org/10.1002/anie.202108170.

Hua, M., Song, J., Huang, X., Liu, H., Fan, H., Wang, W., He, Z., Liu, Z., and Han, B. (2021). Highly efficient oxidative cyanation of aldehydes to nitriles over Se,S,N-*tri*-doped hierarchically porous carbon nanosheets. Angew. Chem. Int. Ed. *60*, 21479–21485. https://doi.org/10.1002/anie.202107996.

Jiang, J., Bai, X., Zhao, X., Chen, W., Yu, T., Li, Y., and Mu, T. (2019). Poly-quasi-eutectic solvents (PQESs): versatile solvents for dissolving metal oxides. Green Chem. *21*, 5571–5578. https://doi.org/10.1039/c9gc02604e.

Jin, C., Nai, J., Sheng, O., Yuan, H., Zhang, W., Tao, X., and Lou, X.W.(D. (2021). Biomass-based materials for green lithium secondary batteries. Energy Environ. Sci. *14*, 1326–1379. https://doi.org/10.1039/d0ee02848g.

Jones, J., Xiong, H., DeLaRiva, A.T., Peterson, E.J., Pham, H., Challa, S.R., Qi, G., Oh, S., Wiebenga, M.H., Hernández, X.I.P., et al. (2016). Thermally stable single-atom platinum-on-ceria catalysts via atom trapping. Science *353*, 150–154. https://doi.org/10.1126/science.aaf8800.

Kang, X., Shang, W., Zhu, Q., Zhang, J., Jiang, T., Han, B., Wu, Z., Li, Z., and Xing, X. (2015). Mesoporous inorganic salts with crystal defects: unusual catalysts and catalyst supports. Chem. Sci. *6*, 1668–1675. https://doi.org/10.1039/c4sc03736g.

Kisszekelyi, P., Hardian, R., Vovusha, H., Chen, B., Zeng, X., Schwingenschlçgl, U., Kupai, J., and Szekely, G. (2020). Selective electrocatalytic oxidation of biomass-derived 5-hydroxymethylfurfural to 2,5-diformylfuran: from mechanistic investigations to catalyst recovery. ChemSusChem *13*, 3127–3136. https://doi.org/10.1002/cssc.202000453.

Kumar, A., Singh, B., Raigond, P., Sahu, C., Mishra, U.N., Sharma, S., and Lal, M.K. (2021). Phytic acid: blessing in disguise, a prime compound required for both plant and human nutrition. Food Res. Int. *142*, 110193. https://doi.org/10.1016/j.foodres.2021.110193.

Kuwahara, Y., Kango, H., and Yamashita, H. (2017). Catalytic transfer hydrogenation of biomass-derived levulinic acid and its esters to γ-valerolactone over sulfonic acid-functionalized UiO-66. ACS Sustainable Chem. Eng. *5*, 1141–1152. https://doi.org/10.1021/acssuschemeng.6b02464.

Li, F., Li, Z., France, L.J., Mu, J., Song, C., Chen, Y., Jiang, L., Long, J., and Li, X. (2018a). Highly efficient transfer hydrogenation of levulinate esters to γ-valerolactone over basic zirconium carbonate. Ind. Eng. Chem. Res. *57*, 10126–10136. https://doi.org/10.1021/acs.iecr.8b00712.

Li, H., Sun, Y., Yuan, Z.Y., Zhu, Y.P., and Ma, T.Y. (2018b). Titanium phosphonate based metal-organic frameworks with hierarchical porosity for enhanced photocatalytic hydrogen evolution. Angew. Chem. Int. Ed. *57*, 3222–3227. https://doi.org/10.1002/anie.201712925.

Li, J., Yang, Y., and Zhang, D. (2019). DFT study of fructose dehydration to 5-hydroxymethylfurfural catalyzed by imidazolium-based ionic liquid. Chem. Phys. Lett. *723*, 175–181. https://doi.org/10.1016/j.cplett.2019.03.047.

Li, M., Xu, F., Li, H., and Wang, Y. (2016). Nitrogen-doped porous carbon materials: promising catalysts or catalyst supports for heterogeneous hydrogenation and oxidation. Catal. Sci. Technol. *6*, 3670–3693. https://doi.org/10.1039/c6cy00544f.

Li, R., Liu, L., and Yang, F. (2014). Removal of aqueous Hg(II) and Cr(VI) using phytic acid doped polyaniline/cellulose acetate composite membrane. J. Hazard Mater. *280*, 20–30. https://doi.org/10.1016/j.jhazmat.2014.07.052.

Li, S., Dong, M., Yang, J., Cheng, X., Shen, X., Liu, S., Wang, Z.-Q., Gong, X.-Q., Liu, H., and Han, B. (2021). Selective hydrogenation of 5-(hydroxymethyl)furfural to 5-methylfurfural over single atomic metals anchored on Nb_2O_5. Nat. Commun. *12*, 584. https://doi.org/10.1038/s41467-020-20878-7.

Lin, X.-Z., Ren, T.-Z., and Yuan, Z.-Y. (2015). Mesoporous zirconium phosphonate materials as efficient water-tolerable solid acid catalysts. Catal. Sci. Technol. *5*, 1485–1494. https://doi.org/10.1039/c4cy01110d.

Liu, X., Min, X., Liu, H., Cao, Y., Liu, Y., Han, M., Sun, Z.-M., and Ji, S. (2020). Efficient conversion of cellulose to 5-hydroxymethylfurfural catalyzed by a cobalt-phosphonate catalyst. Sustain. Energy Fuels *4*, 5795–5801. https://doi.org/10.1039/d0se01006e.

Luo, W., Sankar, M., Beale, A.M., He, Q., Kiely, C.J., Bruijnincx, P.C.A., and Weckhuysen, B.M. (2015). High performing and stable supported nano-alloys for the catalytic hydrogenation of levulinic acid to γ-valerolactone. Nat. Commun. *6*, 6540. https://doi.org/10.1038/ncomms7540.

Ma, Z., Hu, H., Sun, Z., Fang, W., Zhang, J., Yang, L., Zhang, Y., and Wang, L. (2017). Acidic zeolite L as a highly efficient catalyst for dehydration of fructose to 5-hydroxymethylfurfural in ionic liquid. ChemSusChem *10*, 1669–1674. https://doi.org/10.1002/cssc.201700239.

Maschmeyer, T., Luque, R., and Selva, M. (2020). Upgrading of marine (fish and crustaceans) biowaste for high added-value molecules and bio(nano)-materials. Chem. Soc. Rev. *49*, 4527–4563. https://doi.org/10.1039/c9cs00653b.

Mou, H., Wang, J., Yu, D., Zhang, D., Lu, F., Chen, L., Wang, D., and Mu, T. (2019). A facile and controllable, deep eutectic solvent aided strategy for the synthesis of graphene encapsulated metal phosphides for enhanced electrocatalytic overall water splitting. J. Mater. Chem. *7*, 13455–13459. https://doi.org/10.1039/c9ta02304f.

Pfriem, N., Liu, Y., Zahn, F., Shi, H., Haller, G.L., and Lercher, J.A. (2021). Impact of the local concentration of hydronium ions at tungstate surfaces for acid-catalyzed alcohol dehydration. J. Am. Chem. Soc. *143*, 20133–20143. https://doi.org/10.1021/jacs.1c07203.

Sahoo, B., Surkus, A.-E., Pohl, M.-M., Radnik, J., Schneider, M., Bachmann, S., Scalone, M., Junge, K., and Beller, M. (2017). A biomass-derived non-noble cobalt catalyst for selective hydrodehalogenation of alkyl and (hetero)aryl halides. Angew. Chem. Int. Ed. *56*, 11242–11247. https://doi.org/10.1002/anie.201702478.

Sajid, M., Zhao, X., and Liu, D. (2018). Production of 2,5-furandicarboxylic acid (FDCA) from 5-hydroxymethylfurfural (HMF): recent progress focusing on the chemical-catalytic routes. Green Chem. *20*, 5427–5453. https://doi.org/10.1039/c8gc02680g.

Sang, X., Liu, D., Song, J., Wang, C., Nie, X., Shi, G., Xia, X., Ni, C., and Wang, D. (2021). High-efficient liquid exfoliation of 2D metal-organic framework using deep-eutectic solvents. Ultrason. Sonochem. *72*, 105461. https://doi.org/10.1016/j.ultsonch.2021.105461.

Shao, L., Li, Y., Pan, F., Zhang, Z., Liang, S., Wang, Y., Zou, J., and Jiang, Z. (2021). Graphene oxide membranes tuned by metal-phytic acid coordination complex for butanol dehydration. J. Membr. Sci. *638*, 119736. https://doi.org/10.1016/j.memsci.2021.119736.

Smith, E.L., Abbott, A.P., and Ryder, K.S. (2014). Deep eutectic solvents (DESs) and their applications. Chem. Rev. *114*, 11060–11082. https://doi.org/10.1021/cr300162p.

Song, J., Xue, Z., Xie, C., Wu, H., Liu, S., Zhang, L., and Han, B. (2018). Porous, naturally derived hafnium phytate for the highly chemoselective transfer hydrogenation of aldehydes with other reducible moieties. ChemCatChem *10*, 725–730. https://doi.org/10.1002/cctc.201701521.

Song, J., Zhou, B., Zhou, H., Wu, L., Meng, Q., Liu, Z., and Han, B. (2015). Porous zirconium-phytic acid hybrid: a highly efficient catalyst for Meerwein-Ponndorf-Verley reductions. Angew. Chem. Int. Ed. *54*, 9399–9403. https://doi.org/10.1002/anie.201504001.

Sun, S., Liu, S., Yu, F., Zhang, J., Xing, W., and Yu, S. (2022). Reusable deep eutectic solvents for clean ε-caprolactam synthesis under mild conditions. ACS Sustainable Chem. Eng. *10*, 1675–1688. https://doi.org/10.1021/acssuschemeng.1c07613.

Tan, X., Zhao, W., and Mu, T. (2018). Controllable exfoliation of natural silk fibers into nanofibrils by protein denaturant deep eutectic solvent: nanofibrous strategy for multifunctional membranes. Green Chem. *20*, 3625–3633. https://doi.org/10.1039/c8gc01609g.

Wang, G.-H., Hilgert, J., Richter, F.H., Wang, F., Bongard, H.-J., Spliethoff, B., Weidenthaler, C., and Schüth, F. (2014). Platinum-cobalt bimetallic nanoparticles in hollow carbon nanospheres for hydrogenolysis of 5-hydroxymethylfurfural. Nat. Mater. *13*, 294–301. https://doi.org/10.1038/NMAT3872.

Wang, J., Xi, J., Xia, Q., Liu, X., and Wang, Y. (2017). Recent advances in heterogeneous catalytic conversion of glucose to 5-hydroxymethylfurfural via green routes. Sci. China Chem. *60*, 870–886. https://doi.org/10.1007/s11426-016-9035-1.

Wang, S., Nam, G., Li, P., Jang, H., Wang, J., Kim, M.G., Wu, Z., Liu, X., and Cho, J. (2018). Highly active bifunctional oxygen electrocatalysts derived from nickel- or cobalt-phytic acid xerogel for zinc-air batteries. Nanoscale *10*, 15834–15841. https://doi.org/10.1039/c8nr04733b.

Wang, Z., Xie, C., Li, X., Nie, J., Yang, H., and Zhang, Z. (2022). Amberlyst-15 supported zirconium sulfonate as an efficient catalyst for Meerwein-Ponndorf-Verley reductions. Chem. Commun. *58*, 4067–4070. https://doi.org/10.1039/d2cc00157h.

Wu, H., Song, J., Xie, C., Hu, Y., Ma, J., Qian, Q., and Han, B. (2018). Design of naturally derived lead phytate as an electrocatalyst for highly efficient CO_2 reduction to formic acid. Green Chem. *20*, 4602–4606. https://doi.org/10.1039/c8gc02457j.

Xiao, S., Chen, C., Xia, Q., Liu, Y., Yao, Y., Chen, Q., Hartsfield, M., Brozena, A., Tu, K., Eichhorn, S.J., et al. (2021). Lightweight, strong, moldable wood via cell wall engineering as a sustainable structural material. Science *374*, 465–471. https://doi.org/10.1126/science.abg9556.

Xiao, Y., and Song, Y.-F. (2014). Efficient catalytic conversion of the fructose into 5-hydroxymethylfurfural by heteropolyacids in the ionic liquid of 1-butyl-3-methyl imidazolium chloride. Appl. Catal. A Gen. *484*, 74–78. https://doi.org/10.1016/j.apcata.2014.07.014.

Xie, C., Song, J., Wu, H., Hu, Y., Liu, H., Zhang, Z., Zhang, P., Chen, B., and Han, B. (2019). Ambient Reductive amination of levulinic acid to pyrrolidones over Pt nanocatalysts on porous TiO_2 nanosheets. J. Am. Chem. Soc. *141*, 4002–4009. https://doi.org/10.1021/jacs.8b13024.

Xie, H., Zhao, Z.K., and Wang, Q. (2012). Catalytic conversion of inulin and fructose into 5-hydroxymethylfurfural by lignosulfonic acid in ionic liquids. ChemSusChem *5*, 901–905. https://doi.org/10.1002/cssc.201100588.

Xu, C., Paone, E., Rodríguez-Padrón, D., Luque, R., and Mauriello, F. (2020). Recent catalytic routes for the preparation and the upgrading of biomass derived furfural and 5-hydroxymethylfurfural. Chem. Soc. Rev. *49*, 4273–4306. https://doi.org/10.1039/d0cs00041h.

Xue, Z., Jiang, J., Li, G., Zhao, W., Wang, J., and Mu, T. (2016a). Zirconium-cyanuric acid coordination polymer: highly efficient catalyst for conversion of levulinic acid to γ-valerolactone. Catal. Sci. Technol. *6*, 5374–5379. https://doi.org/10.1039/c5cy02215k.

Xue, Z., Zhang, Y., Li, G., Wang, J., Zhao, W., and Mu, T. (2016b). Niobium phytate prepared from phytic acid and $NbCl_5$: a highly efficient and heterogeneous acid catalyst. Catal. Sci. Technol. *6*, 1070–1076. https://doi.org/10.1039/c5cy01123j.

Yang, D., Gaggioli, C.A., Ray, D., Babucci, M., Gagliardi, L., and Gates, B.C. (2020). Tuning catalytic sites on Zr_6O_8 metal-organic framework nodes via ligand and defect chemistry probed with *tert*-butyl alcohol dehydration to isobutylene. J. Am. Chem. Soc. *142*, 8044–8056. https://doi.org/10.1021/jacs.0c03175.

Yang, X.-F., Wang, A., Qiao, B., Li, J., Liu, J., and Zhang, T. (2013). Single-atom catalysts: a new Frontier in heterogeneous catalysis. Acc. Chem. Res. *46*, 1740–1748. https://doi.org/10.1021/ar300361m.

Yu, D., Xue, Z., and Mu, T. (2021). Eutectics: formation, properties, and applications. Chem. Soc. Rev. *50*, 8596–8638. https://doi.org/10.1039/d1cs00404b.

Zhang, M., Li, Z., Xin, X., Zhang, J., Feng, Y., and Lv, H. (2020). Selective valorization of 5-hydroxymethylfurfural to 2,5-diformylfuran using atmospheric O_2 and $MAPbBr_3$ perovskite under visible light. ACS Catal. *10*, 14793–14800. https://doi.org/10.1021/acscatal.0c04330.

Zhang, X., Zhou, X.-Y., Cheng, X.-W., and Tang, R.-C. (2018). Phytic acid as an eco-friendly flame retardant for silk/wool blend: a comparative study with fluorotitanate and fluorozirconate. J. Clean. Prod. *198*, 1044–1052. https://doi.org/10.1016/j.jclepro.2018.07.103.

Zhao, H., Holladay, J.E., Brown, H., and Zhang, Z.C. (2007). Metal chlorides in ionic liquid solvents convert sugars to 5-hydroxymethylfurfural. Science *316*, 1597–1600. https://doi.org/10.1126/science.1141199.

Zhou, T., Du, Y., Wang, D., Yin, S., Tu, W., Chen, Z., Borgna, A., and Xu, R. (2017). Phosphonate-based metal-organic framework derived Co-P-C hybrid as an efficient electrocatalyst for oxygen evolution reaction. ACS Catal. *7*, 6000–6007. https://doi.org/10.1021/acscatal.7b00937.

STAR★METHODS

KEY RESOURCES TABLE

REAGENT	SOURCE	IDENTIFIER
Phytic acid (45 wt% aqueous solution)	J&K Scientific Co., Ltd (China)	388440
Zirconium dichloride oxide octahydrate (98%)	J&K Scientific Co., Ltd (China)	251259
Zirconium(IV) oxide (99%)	J&K Scientific Co., Ltd (China)	616897
N,N-dimethylformamide	J&K Scientific Co., Ltd (China)	910304
5-Hydroxymethylfurfural (98%)	J&K Scientific Co., Ltd (China)	072925
Isopropanol (99.5%)	Beijing InnoChem Science & Technology Co., Ltd (China)	A53496
Acetonitrile (99.9%)	Beijing InnoChem Science & Technology Co., Ltd (China)	A62556
Methanol (99.5%)	Beijing InnoChem Science & Technology Co., Ltd (China)	A73501
Ethylene glycol (99%)	Beijing InnoChem Science & Technology Co., Ltd (China)	A82640
Urea (99%)	Beijing InnoChem Science & Technology Co., Ltd (China)	A93228
Cyclohexanol (99%)	Alfa (China)	A17576
γ-Valerolactone (98%)	Alfa (China)	A18872
D-Fructose (99%)	Alfa (China)	A17718
Sucrose (99%)	Alfa (China)	A15583
D-(+)-Glucose (99%)	Alfa (China)	A16828
Ethyl levulinate (98%)	Alfa (China)	A15001
Inulin from dahlia tubers	Aladdin (China)	I111088-25g
1-Butyl-3-methylimidazolium chloride ([Bmim]Cl) (99.9%)	Lanzhou Greenchem ILs, LICP, CAS, China (Lanzhou, China)	N/A
Diethyl ether (A.R.)	Beijing Chemical Reagent Company	N/A

RESOURCE AVAILABILITY

Lead contact

Further information and requests for resources should be directed to and will be fulfilled by the lead contact, Jinliang Song (songjl_2021@gdut.edu.cn).

Materials availability

This study did not generate new unique reagents.

Data and code availability

- All data reported in this paper will be shared by the lead contact upon request.
- This paper does not report original code.
- Any additional information required to reanalyze the data reported in this work is available from the lead contact upon reasonable request.

METHOD DETAILS

Preparation of the desired DES (EG:Urea-2:1)

In a typical route, ethylene glycol (2 mol) and urea (1 mol) were added into a flask of 1 L. Then, the flask was placed into an oil bath at 60 °C. After the mixture completely became a liquid, the procedure was stopped. Finally, the obtained EG:Urea-2:1 was stored in a desiccator for subsequent applications.

Synthesis of Zr-Phy-*DES*, Zr-Phy-*EG*, and Zr-Phy-*DMF*

In a typical procedure, $ZrOCl_2 \cdot 8H_2O$ (15 mmol, dissolved in 5 mL water) and phytic acid (5 mmol) were added into the EG:Urea-2:1 (100 mL) in a polyurethane reactor (150 mL), and the mixture was stirred for 2 h. Subsequently, the reactor was sealed and placed into an oven with a temperature of 150 °C for 24

h. After the above step, the mixture in the reactor was transformed into a beaker (1 L) containing 600 mL water. The precipitation was collected by centrifugation and was thoroughly washed with deionized water to remove the residual EG and urea. Finally, the precipitation was dried *via* the freeze-drying process to obtain the desired Zr-Phy-*DES*. The route to synthesize Zr-Phy-*EG* and Zr-Phy-*DMF* was similar with that of synthesizing Zr-Phy-*DES* except that the used solvents were EG and DMF, respectively.

Catalyst characterization

FT-IR spectra were recorded on Bruker Tensor 27 IR spectrometer using the KBr pellet method. XPS measurements were carried out on an ESCAL Lab 220i-XL specrometer under a pressure of $\sim 3 \times 10^{-9}$ mbar (1 mbar = 100 Pa). XRD measurements were performed on an X-ray diffractometer (D/MAX-RC, Japan) at 40 kV and 200 mA with Cu Kα (λ = 0.154 nm) radiation. TEM images were achieved on a TEM JeoL-1011 with an accelerating voltage of 120 kV. SEM images were obtained on a Hitachi S-4800 Scanning Electron Microscope operated at 15 kV. Elemental mappings of Zr-Phy-DES were recorded using a JEOL-2100F high resolution of transmission electron microscopy (HR-TEM). The content of Zr was detected by ICP-AES (VISTA-MPX). N_2 adsorption-desorption isotherms were obtained on the Micromeritics ASAP 2020 V3.00H (USA) surface area analyzer at 77 K at high vacuum. Temperature-programmed desorption of ammonia (NH_3-TPD) and temperature-programmed desorption of carbon dioxide (CO_2-TPD) were conducted on Micromeritics' AutoChem 2950 HP Chemisorption Analyzer.

Dehydration of various carbohydrates

In a typical route, the carbohydrate (0.1 g), the desired catalyst (0.1 g) and [Bmim]Cl (1 g) were added into a flask of 10 mL, and the mixture was stirred at 100 °C for a desired reaction time. After the reaction, the flask was cooled to room temperature quickly by ice water. The conversion of the reactant was analyzed by HPLC using an external standard method with Hypersil NH_2 5 μm column, Shimadzu LC-15C pump, and Shimadzu RID-10A detectors at 35°C, and acetonitrile/water solution (75/25 V/V) was employed as the mobile phase at a flow rate of 0.8 mL/min. Meanwhile, the actual amount of HMF was also determined by HPLC using an external standard method with Shimadzu LC-15C pump, Shimadzu UV-Vis SPD-15C detector at 282.0 nm, and a Supelcosil LC-18 5im column at 35°C, and methanol/water solution (50/50 V/V) was used as the mobile phase at a flow rate of 0.8 mL/min.

The used Zr-Phy-*DES* was recovered by centrifugation after each catalytic cycle. After being washed using water (3 × 5 mL), the recovered Zr-Phy-*DES* was dried at 80 °C with a time of 6 h under vacuum. Then, the recovered Zr-Phy-*DES* was reused for the next catalytic run by adding new fructose and [Bmim]Cl.

In the experiments to determine the reusability of the whole Zr-Phy-*DES*/[Bmim]Cl catalytic system, water (1 mL) was added into the reaction system after the reaction. Subsequently, diethyl ether (20 × 5 mL) was employed to extract HMF from the reaction system. When the HMF was completely extracted, which could be monitored by HPLC, most of the water in the catalytic system was firstly removed by rotary evaporation at 60 °C with a time of 4 h, and then the Zr-Phy-*DES*/[Bmim]Cl system was freeze-dried to remove the remained water of small amount for 12 h. Finally, the Zr-Phy-*DES*/[Bmim]Cl catalytic system was used directly for the next run by adding new fructose, and the amount sum of the added new fructose and the remained fructose was kept as 0.1 g.

MPV reduction of EL

In a typical experiment, EL (1 mmol), isopropanol (5 g) and the desired catalyst (0.2 g) were added into an autoclave of 22 mL. After the autoclave was sealed, it was placed into an air oven with a constant temperature of 130 °C. After the reaction was conducted for a desired reaction time, the autoclave was placed into ice water to quickly stop the reaction. Finally, the amounts of the unreacted reactant and the generated products were determined by gas chromatography (GC) using cyclohexanol as the internal standard, and the GC instrument (Agilent 6820) was equipped with a flame-ionized detector and an HP-5MS capillary column (0.25 mm in diameter, 30 m in length).

To recycle Zr-Phy-*DES*, the used catalyst was separated via centrifugation, and washed with isopropanol (5 × 5 mL). After being dried at 60 °C under vacuum for 6 h, the recovered Zr-Phy-*DES* was directly reused in the next catalytic cycle.